sinoatrial node. We hypothesized that the medetomidine-induced vagal activation might be impaired in SHR compared to WKY. To test the hypothesis, we applied a cardiac microdialysis technique to the rat left ventricular free wall and compared the effects of intravenous administration of medetomidine on myocardial interstitial ACh levels in WKY and SHR. Furthermore, to examine whether peripheral vagal control of ACh release is impaired in SHR, myocardial interstitial ACh release in response to electrical vagal stimulation was examined in WKY and SHR.

Materials and methods

Surgical preparation

Animal care was conducted in strict accordance with the *Guiding Principles for the Care and Use of Animals in the Field of Physiological Sciences*, which has been approved by the Physiological Society of Japan. All protocols were reviewed and approved by the Animal Subject Committee of National Cerebral and Cardiovascular Center.

Two main protocols were conducted in male WKY (300–400 g) and SHR (320–380 g) as described in '*Protocols*' below. Each rat was anaesthetized with an intraperitoneal injection (2 mL kg^{-1}) of a mixture of urethane (250 mg mL^{-1}) and α-chloralose (40 mg mL^{-1}), and mechanically ventilated with oxygen-enriched room air. Venous catheters were inserted into bilateral external jugular veins. One venous catheter was used for continuous infusion of a 20-fold diluted solution of the above anaesthetic mixture (2–3 mL kg^{-1} h^{-1}) and Ringer's solution (5–6 mL kg^{-1} h^{-1}), and the other for the injection of test drugs. An arterial catheter was inserted into the right common carotid artery to measure the arterial pressure (AP) and HR. In Protocol 2, the vagi were sectioned at the neck, and a pair of stainless steel wire electrodes (Bioflex wire, AS633; Cooner Wire, Chatsworth, CA, USA) was attached to the distal segment of the sectioned nerve bilaterally for efferent vagal nerve stimulation. The nerves and electrodes were secured and insulated with silicone glue (Kwik-Sil; World Precision Instruments, Sarasota, FL, USA). The animal was then placed in a lateral position, and the left third to fifth ribs were partially resected to expose the heart. The pericardium was incised and a dialysis probe was implanted into the lateral free wall of the left ventricle as shown in Figure 1. Body temperature of the animal was maintained at around 38 °C by a heating pad and a lamp. At the end of the experiment, a postmortem examination confirmed that the dialysis membrane was not exposed into the left ventricular cavity.

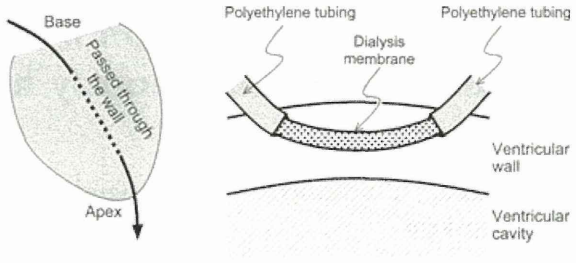

Figure 1 Schematic diagram of dialysis probe implantation. The transverse dialysis probe was implanted within the left ventricular free wall.

Dialysis technique

Dialysate concentration of ACh was measured as an index of myocardial interstitial ACh level. The materials and properties of the dialysis probe have been described previously (Akiyama *et al.* 1994). Briefly, we designed a straight, transverse dialysis probe consisting of a dialysis fibre (length, 6 mm; outer diameter, 310 μm; inner diameter, 200 μm; PAN-1200, 50 000-Da molecular weight cut-off; Asahi Chemical, Osaka, Japan) glued at both ends to polyethylene tubes (length, 25 cm; outer diameter, 500 μm; inner diameter, 200 μm). The dialysis probe was perfused with Ringer's solution containing a cholinesterase inhibitor eserine (100 μmol L^{-1}; Wako Pure Chemical, Osaka, Japan). Dialysate sampling was started from 2 h after probe implantation. In Protocol 1, the perfusion rate was set at 1 μL min^{-1}. Each sampling period was 20 min, which yielded a sample volume of 20 μL. A time lag of 10 min was allowed between actual dialysate sampling and collection of the sample into a tube, taking into account the dead space between the dialysis membrane and collecting tube. In Protocol 2 and in the supplemental protocol, to reduce possible tachyphylaxis induced by constant vagal nerve stimulation, the sampling period was halved to 10 min, while the perfusion rate was doubled to 2 μL min^{-1}. The time lag between actual dialysate sampling and sample collection was 5 min. The concentration of ACh in the dialysate was measured using a high-performance liquid chromatography system with electrochemical detection (Eicom, Kyoto, Japan) adjusted to measure low levels of ACh (Shimizu *et al.* 2009, 2012; Kawada *et al.* 2009, 2010).

Protocols

Protocol 1 ($n = 7$ each for WKY and SHR): After collecting a baseline dialysate sample for 20 min, medetomidine (0.1 mg kg^{-1}; Orion Pharma, Espoo, Finland) was injected intravenously via the jugular vein. Medetomidine initially increases AP by

vasoconstriction via its peripheral α_2-adrenergic effect, then decreases AP as time elapses by sympathetic inhibition via its central α_2-adrenergic effect (Sinclair 2003). After allowing a 10-min stabilization period after medetomidine administration, dialysate was sampled for 20 min. Next, to avoid hypotension induced by medetomidine, intravenous infusion of an α_1-adrenergic agonist phenylephrine (250 μg kg^{-1} h^{-1}; Kowa Pharmaceuticals, Nagoya, Japan) was started simultaneous to injection of an additional dose of medetomidine (0.1 mg kg^{-1}). After allowing 10-min stabilization, dialysate was sampled for 20 min.

Protocol 2 (n = 6 for WKY and SHR each): This protocol was performed under vagotomized conditions. Before collecting a baseline dialysate sample, bilateral vagi were stimulated (20 Hz, 5 V, 2-ms pulse width) for 10 min twice with an intervening interval of 10 min in order to establish stable stimulatory conditions. A supramaximal amplitude was used in stimulation, and increasing the amplitude beyond 5 V did not induce further bradycardic response. Baseline dialysate was then sampled for 10 min. Thereafter, the vagi were stimulated for 10 min, and the corresponding dialysate sample was collected for 10 min. Next, vagal nerve stimulation was discontinued, and medetomidine (0.1 mg kg^{-1}) was injected intravenously via the jugular vein. After 10-min stabilization, dialysate was sampled for 10 min. Finally, the vagi were again stimulated for 10 min, and the corresponding dialysate sample was collected for 10 min.

Supplemental protocol (n = 5, WKY): To determine the source of ACh measured by the cardiac microdialysis, we implanted one or two dialysis probes into the left ventricular free wall in vagotomized rats. Dialysate samples were collected for 10 min before and during bilateral vagal stimulation (20 Hz, 5V, 2-ms pulse width) under control conditions. The perfusate was then replaced with the one containing 1 mmol L^{-1} of hexamethonium bromide (Wako Pure Chemical) (Akiyama *et al.* 2004). After 30-min stabilization, dialysate samples were collected before and during bilateral vagal stimulation. Finally, hexamethonium bromide was injected intravenously (60 mg mL^{-1}, bolus). After 10-min stabilization, dialysate samples were collected before and during bilateral vagal stimulation.

Statistical analysis

All data are presented as mean and SE. Data of mean HR and AP during intravenous pharmacological interventions were measured after a 10-min stabilization period. Data of mean HR and AP during vagal stimulation were measured at 5 min of vagal stimulation. In Protocol 1 and in the supplemental protocol, changes in dialysate ACh, HR and AP were analysed using repeated-measures analysis of variance (ANOVA) followed by Tukey's test for all pairwise comparisons (Glantz 2002). In Protocol 2, changes in dialysate ACh, HR and AP were analysed using repeated-measures two-way ANOVA with vagal nerve stimulation as one factor and medetomidine as the other. For ACh data, because the variance of measured ACh levels increased as the mean increased, statistical analyses were performed after logarithmic conversion (Snedecor & Cochran 1989). The AP and HR data were analysed without logarithmic conversion. Changes in ACh and HR in response to vagal nerve stimulation in WKY and SHR were compared by unpaired t-test. In all statistical analyses, differences were considered significant when $P < 0.05$.

Results

Figure 2 illustrates the results of Protocol 1. In the WKY group, medetomidine alone significantly increased myocardial interstitial ACh level from 2.4 ± 0.6 to 4.2 ± 1.3 nmol L^{-1} ($P < 0.05$) and decreased HR ($P < 0.05$) without significantly affecting AP. Medetomidine combined with phenylephrine significantly increased ACh to 5.8 ± 2.0 nmol L^{-1} ($P < 0.01$) and decreased HR ($P < 0.05$) compared to baseline levels, but did not change both parameters compared to medetomidine alone. Medetomidine combined with phenylephrine resulted in a significant elevation in AP ($P < 0.01$). In the SHR group, medetomidine alone did not affect ACh significantly (from 2.5 ± 0.7 to 2.7 ± 0.7 nmol L^{-1}), although it decreased HR ($P < 0.05$). Medetomidine alone caused significant hypotension ($P < 0.01$). Although medetomidine combined with phenylephrine prevented medetomidine-induced hypotension, it did not significantly affect the ACh level (3.2 ± 0.8 nmol L^{-1}). HR observed after administering medetomidine combined with phenylephrine was not significantly different from baseline.

Figure 3 illustrates the results of Protocol 2. Electrical vagal nerve stimulation increased the ACh levels in both WKY (from 1.0 ± 0.4 to 2.9 ± 0.9 nmol L^{-1}) and SHR (from 0.9 ± 0.2 to 2.2 ± 0.4 nmol L^{-1}) under control conditions. In the WKY group, vagal stimulation significantly increased ACh and decreased HR but did not affect AP. Medetomidine significantly decreased HR and AP but did not significantly change ACh. No significant interaction effect was detected by two-way ANOVA, indicating that medetomidine did not affect the vagal nerve stimulation–induced ACh or HR response. In the SHR group, vagal nerve stimulation significantly increased ACh and decreased HR and AP. Medetomidine significantly decreased HR and AP but

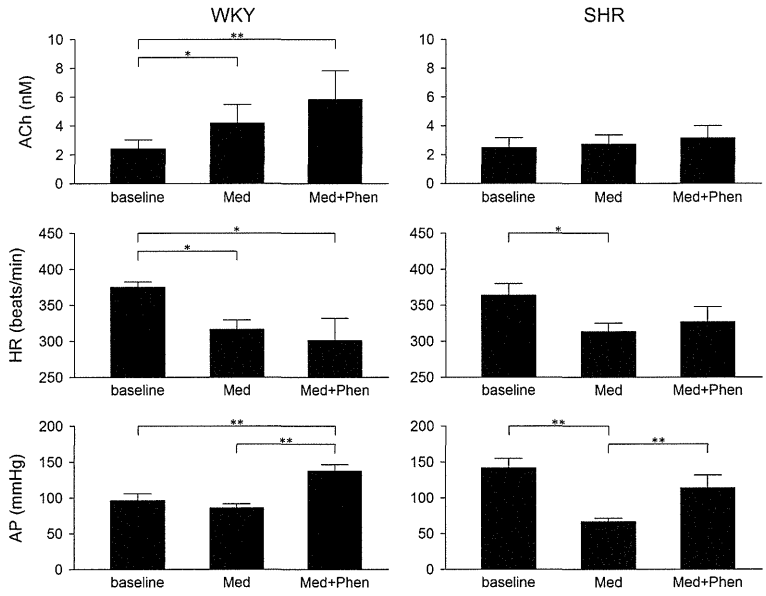

Figure 2 Effects of intravenous medetomidine (Med) alone and medetomidine combined with phenylephrine (Med+Phen) on myocardial interstitial acetylcholine (ACh) level, heart rate (HR) and arterial pressure (AP) in Wistar–Kyoto rats (WKY) and spontaneously hypertensive rats (SHR). Data are presented as mean and SE. $^{*}P < 0.05$ and $^{**}P < 0.01$ by Tukey's test after repeated-measures one-way analysis of variance (ANOVA).

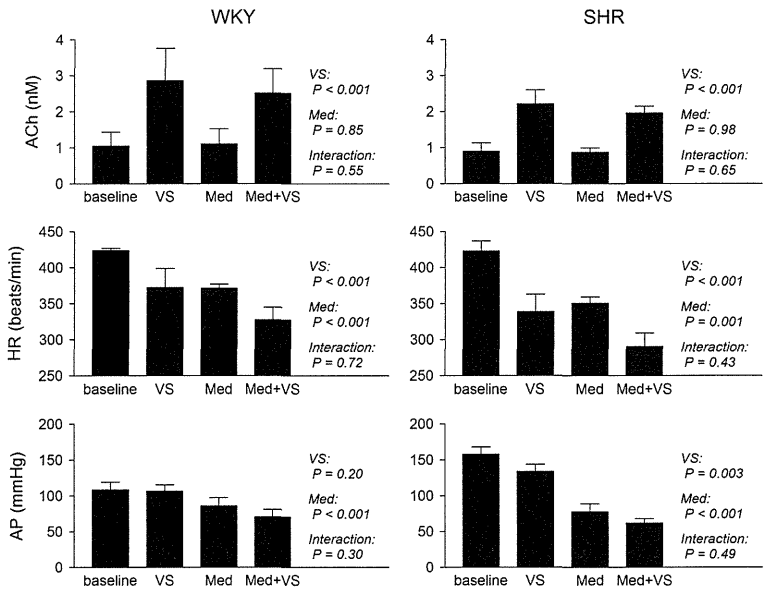

Figure 3 Effects of electrical vagal nerve stimulation (VS), intravenous medetomidine (Med) and vagal nerve stimulation with medetomidine pretreatment (Med+VS) on myocardial interstitial acetylcholine (ACh) level, heart rate (HR) and arterial pressure (AP) in Wistar–Kyoto rats (WKY) and spontaneously hypertensive rats (SHR). Data are presented as mean and SE. The *P* values represent the results of repeated-measures two-way analysis of variance (ANOVA).

did not significantly change ACh. No significant interaction effect was detected by two-way ANOVA, indicating that medetomidine did not affect the vagal nerve stimulation–induced ACh, HR or AP response. Under control conditions before medetomidine administration, the increase in ACh by vagal nerve stimulation did not differ significantly between WKY and SHR (ΔACh: 1.8 ± 0.6 vs. 1.3 ± 0.3 nmol L^{-1}, $P = 0.46$). The HR decrease induced by vagal nerve stimulation tended to be greater in SHR than in WKY (ΔHR: −51 ± 20 vs. −101 ± 12 beats min^{-1}, $P = 0.06$).

In the supplemental protocol (seven dialysis probes from five WKY rats), electrical vagal stimulation increased the myocardial interstitial ACh level from 0.7 ± 0.2 to 3.6 ± 1.2 nmol L^{-1} ($P < 0.01$) under control conditions (Fig. 4, top). Electrical vagal stimulation increased the myocardial interstitial ACh level from 0.6 ± 0.2 to 3.1 ± 1.1 nmol L^{-1} ($P < 0.01$) during the local administration of hexamethonium through the dialysis probe. There was no statistically significant difference in the vagal stimulation–induced ACh release between the control and local hexamethonium conditions. After the intravenous administration of hexamethonium, electrical vagal stimulation did not increase the myocardial interstitial ACh level (0.8 ± 0.3 to 0.7 ± 0.2 nmol L^{-1}). The intravenous administration of hexamethonium reduced prestimulation HR and abolished the vagal stimulation–induced

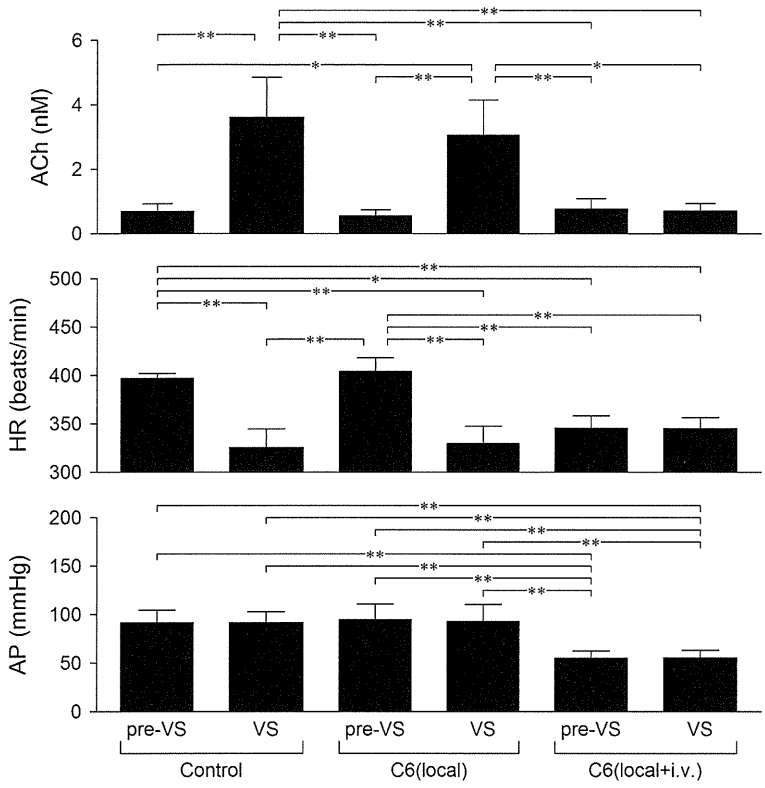

Figure 4 Effects of local administration of hexamethonium bromide [C6(local)] and intravenous administration of hexamethonium bromide [C6(local+i.v.)] on the electrical vagal stimulation–induced ACh release in five Wistar–Kyoto rats. For ACh data, seven dialysate samples from the five rats were analysed. Because intravenous administration of hexamethonium completely blocked the vagal stimulation–induced ACh release, the ACh measured by cardiac microdialysis was mainly originated from the postganglionic vagal nerves. The failure of local administration of hexamethonium to block the ACh release suggests that vagal ganglia were not present nearby the dialysis fibre. Data are presented as mean and SE. $P < 0.05$ and $P < 0.01$ by Tukey's test after repeated-measures one-way analysis of variance (ANOVA).

bradycardia (Fig. 4, middle). The intravenous administration of hexamethonium also reduced AP irrespective of vagal stimulation (Fig. 4, bottom).

Discussion

The present study demonstrated that intravenous medetomidine increased left ventricular myocardial interstitial ACh levels in WKY but not in SHR, indicating that medetomidine-induced central vagal activation was impaired in SHR. Vagal nerve stimulation increased the ACh levels in both WKY and SHR, suggesting that the peripheral vagal control of ACh release was preserved in SHR. The results of the supplemental protocol indicated that the myocardial interstitial ACh measured by cardiac microdialysis in the rat left ventricle was mainly derived from the postganglionic vagal nerve.

Effects of medetomidine on myocardial interstitial ACh release

Medetomidine is a racemic mixture of dexmedetomidine and levomedetomidine. Because levomedetomidine has been shown to be physiologically inert (Kuusela *et al.* 2000), the effects of medetomidine are mostly attributable to those of dexmedetomidine. As expected based on our previous study (Shimizu *et al.* 2012), medetomidine increased myocardial interstitial ACh level significantly in the left ventricle in WKY (Fig. 2). Because α_2-adrenergic receptors are densely distributed in the dorsal motor nucleus of the vagus and nucleus tractus solitarius (Robertson & Leslie 1985), α_2-adrenergic agonists probably activate the cardiac vagal nerve through the action on these brainstem areas. In addition, recent papers indicate that α_2-adrenergic receptor activation inhibits GABAergic neurotransmission in the nucleus ambiguus so as to increase the activity of premotor cardioinhibitory vagal neurones (Philbin *et al.* 2010), and α_1-adrenergic receptor activation facilitates GABAergic and glycinergic neurotransmission so as to reduce the activity of cardioinhibitory vagal neurones (Boychuk *et al.* 2011). In contrast to WKY, the same dose of medetomidine did not affect the ACh level in SHR, suggesting impairment of α_2-adrenergic stimulation–induced central vagal activation in SHR. Although HR was reduced by medetomidine in both WKY and SHR, no significant change in ACh level and significant hypotension observed after medetomidine injection in SHR suggest that the bradycardia observed in SHR was primarily because of sympathetic inhibition rather than vagal activation.

Intravenous medetomidine had a greater hypotensive effect in SHR than in WKY, indicating that hypertension in SHR was dependent on sympathetic

Acta Physiologica © 2012 Scandinavian Physiological Society, doi: 10.1111/j.1748-1716.2012.02439.x

nerve activity. The reduction in peripheral vascular resistance owing to sympathetic suppression may account for the significant hypotension induced by medetomidine in SHR. To exclude the possibility that medetomidine-induced hypotension in SHR prevented ACh release because of the deactivation of the arterial baroreflex, AP was maintained by continuous infusion of phenylephrine. The same dose of phenylephrine resulted in comparable AP elevation in both groups (WKY: $\Delta AP = 47 \pm 16$ and SHR: $\Delta AP = 52 \pm 11$ mmHg), consistent with a previous study (Jablonskis & Howe 1994). Despite the maintenance of AP above 110 mmHg in SHR, medetomidine failed to increase the ACh levels in these rats. The arterial baroreflex function is known to reset to a higher input pressure range in SHR (Nosaka & Wang 1972); therefore, the AP elevation may not have been sufficiently high to evoke a significant baroreflex-mediated vagal activation in SHR. While increasing the dose of phenylephrine could further increase AP in SHR, there is a concern of a possible confounding effect as follows. In the superfused rat atrium, α_1-adrenergic stimulation has been shown to suppress ACh outflow in response to K^+ exposure (McDonough *et al.* 1986). Such presynaptic inhibition via the α_1-adrenergic mechanism might counteract the medetomidine-induced ACh release when the dose of phenylephrine is increased. Further studies are needed to determine whether a lack of arterial baroreceptor input signal after medetomidine injection can totally explain the loss of vagal activation in SHR.

Effects of electrical vagal stimulation on myocardial interstitial ACh release

In Protocol 2, which was conducted under vagotomized conditions, medetomidine alone did not increase myocardial interstitial ACh level in WKY, suggesting that medetomidine increased the ACh level in Protocol 1 by centrally activating the cardiac vagal nerve and not by directly exciting parasympathetic ganglia or vagal nerve terminals. These results are supported by a previous study from our laboratories, in which intravenous medetomidine did not affect the vagal nerve stimulation–induced ACh release in rabbit right atrium (Shimizu *et al.* 2012). Pretreatment with medetomidine did not significantly modify the vagal nerve stimulation–induced ACh release in WKY, which agrees with previous experimental results using superfused rat atrium, in which α_1-adrenergic but not α_2-adrenergic stimulation reduced the K^+-evoked ACh outflow (McDonough *et al.* 1986).

Electrical vagal nerve stimulation induced the myocardial interstitial ACh release in SHR similar to that in WKY (Fig. 3), suggesting that peripheral vagal control of ACh release was preserved in SHR. Although *ex vivo* HR response to vagal nerve stimulation is attenuated in SHR compared to WKY in an isolated atrial/right vagus preparation (Heaton *et al.* 2007), *in vivo* HR response to vagal nerve stimulation is not different between WKY and SHR or is enhanced in SHR than in WKY depending on the age investigated (Ferrari *et al.* 1992, Minami & Head 2000, Masuda 2000). In the present study, HR response to vagal nerve stimulation tended to be enhanced in SHR, consistent with previous *in vivo* investigations. Furthermore, because medetomidine did not significantly modulate the vagal nerve stimulation–induced ACh release in SHR, the lack of ACh response to medetomidine seen in Protocol 1 may be a centrally derived defect. Loss of cardiac vagal preganglionic neurones in adult SHR may be related to the impaired central vagal activation by medetomidine (Corbett *et al.* 2007).

Vagal nerve stimulation had no significant effect on AP in WKY. An increase in the stroke volume occurs in the closed circulatory system and may compensate for the decrease in the number of heartbeat to keep cardiac output. The finding is consistent with a previous study showing that moderate vagal nerve stimulation does not significantly affect the arterial baroreflex-mediated AP regulation (Kawada *et al.* 2011). In contrast, vagal nerve stimulation decreased AP significantly in SHR irrespective of the presence of medetomidine. Because there may be no major innervation of the vagal nerve over the peripheral vasculature, the reduction in AP induced by vagal stimulation observed in SHR is likely to be cardiac origin. For instance, vagal nerve stimulation can reduce ventricular contractility in the presence of a sympathetic tone (Nakayama *et al.* 2001). Because sympathetic nerve activity is higher in SHR than in WKY (Tsunoda *et al.* 2000), vagal nerve stimulation could decrease AP by reducing ventricular contractility before the administration of medetomidine. On the other hand, because medetomidine might have suppressed sympathetic nerve activity, interaction between the vagal and sympathetic systems cannot explain the vagal nerve stimulation–induced hypotension in SHR after medetomidine administration. There is a positive force–frequency relationship (FFR) in large animals such as dogs (Mitchell *et al.* 1963, Kambayashi *et al.* 1992). In rabbits, vagal nerve stimulation decreases ventricular contractility mainly through its negative chronotropic effect, that is, via a positive FFR (Matsuura *et al.* 1997). In contrast, the FFR may be negative in the physiological HR range (200–500 beats min^{-1}) in rats (Nalivaiko *et al.* 2010). Therefore, the FFR alone might have operated to increase the ventricular contractility during bradycardia in rats. Further investigations

are needed to identify the mechanisms involved in the hypotensive effects of vagal nerve stimulation observed in SHR.

Limitation

Several limitations to the present study need to be addressed. First, to avoid the degradation of ACh, an acetylcholinesterase inhibitor eserine was added to the perfusate. Although myocardial interstitial ACh levels measured by cardiac microdialysis have been shown to reflect changes in the ACh kinetics induced by pharmacological or pathological interventions (Kawada *et al.* 2000, 2001), the results have to be interpreted carefully. Second, because of the different perfusion rates, the ACh levels obtained in Protocols 1 and 2 cannot be compared directly. For instance, the lower baseline ACh levels in Protocol 2 compared to Protocol 1 are not necessarily the results of vagotomy. Third, we measured myocardial interstitial ACh levels in the left ventricle and not in the right atrium near the sinoatrial node. Although we assumed that changes in ACh level account for the alterations in HR induced by the vagal nerve, changes in ACh level in the ventricle may not be proportional to changes in the sinoatrial node. Finally, the experiments were carried out on rats at an age when hypertension in SHR is well established. Further studies are required to determine whether the abnormality of central vagal activation in SHR occurs at an earlier age before hypertension is developing.

Conclusion

Alpha$_2$-adrenergic stimulation induced the central vagal activation in WKY, but this mechanism was impaired in SHR. In addition to abnormal sympathetic control, vagal control by the central nervous system may be impaired in SHR. On the other hand, peripheral vagal control of ACh release and HR response may be preserved in SHR.

Conflict of interest

The authors declared no conflict of interest.

This study was supported by Health and Labour Sciences Research Grants (H19-nano-Ippan-009, H20-katsudo-Shitei-007 and H21-nano-Ippan-005) from the Ministry of Health, Labour and Welfare of Japan; and by the Grant-in-Aid for Scientific Research (23592319, 23·01705) promoted by the Ministry of Education, Culture, Sports, Science and Technology of Japan; and by the Industrial Technology Research Grant Program from the New Energy and Industrial Technology Development Organization (NEDO) of Japan.

References

Akiyama, T., Yamazaki, T. & Ninomiya, I. 1994. In vivo detection of endogenous acetylcholine release in cat ventricles. *Am J Physiol* **266**, H854–H860.

Akiyama, T., Yamazaki, T., Mori, H. & Sunagawa, K. 2004. Simultaneous monitoring of acetylcholine and catecholamine release in the in vivo rat adrenal medulla. *Neurochem Int* **44**, 497–503.

Boychuk, C.R., Bateman, R.J., Philbin, K.E. & Mendelowitz, D. 2011. α_1-adrenergic receptors facilitate inhibitory neurotransmission to cardiac vagal neurons in the nucleus ambiguus. *Neuroscience* **193**, 154–161.

Corbett, E.K., Mary, D.A., McWilliam, P.N. & Batten, T.F. 2007. Age-related loss of cardiac vagal preganglionic neurones in spontaneously hypertensive rats. *Exp Physiol* **92**, 1005–1013.

Ferrari, A.U., Daffonchio, A., Franzelli, C. & Mancia, G. 1992. Cardiac parasympathetic hyperresponsiveness in spontaneously hypertensive rats. *Hypertension* **19**, 653–657.

Glantz, S.A. 2002. *Primer of Biostatistics*, 5th edn, McGraw-Hill, New York.

Heaton, D.A., Li, D., Almond, S.C., Dawson, T.A., Wang, L., Channon, K.M. & Paterson, D.J. 2007. Gene transfer of neuronal nitric oxide synthase into intracardiac ganglia reverses vagal impairment in hypertensive rats. *Hypertension* **49**, 380–388.

Jablonskis, L.T. & Howe, P.R. 1994. Lack of influence of circulating adrenaline on blood pressure in normotensive and hypertensive rats. *Blood Press* **3**, 112–119.

Kambayashi, M., Miura, T., Oh, B.H., Rockman, H.A., Murata, K. & Ross, J. Jr 1992. Enhancement of the force-frequency effect on myocardial contractility by adrenergic stimulation in conscious dogs. *Circulation* **86**, 572–580.

Kawada, T., Yamazaki, T., Akiyama, T., Sato, T., Shishido, T., Inagaki, M., Takaki, H., Sugimachi, M. & Sunagawa, K. 2000. Differential acetylcholine release mechanisms in the ischemic and non-ischemic myocardium. *J Mol Cell Cardiol* **32**, 405–414.

Kawada, T., Yamazaki, T., Akiyama, T., Shishido, T., Inagaki, M., Uemura, K., Miyamoto, T., Sugimachi, M., Takaki, H. & Sunagawa, K. 2001. In vivo assessment of acetylcholine-releasing function at cardiac vagal nerve terminals. *Am J Physiol Heart Circ Physiol* **281**, H139–H145.

Kawada, T., Akiyama, T., Shimizu, S., Kamiya, A., Uemura, K., Li, M., Shirai, M. & Sugimachi, M. 2009. Detection of endogenous acetylcholine release during brief ischemia in the rabbit ventricle: a possible trigger for ischemic preconditioning. *Life Sci* **85**, 597–601.

Kawada, T., Akiyama, T., Shimizu, S., Kamiya, A., Uemura, K., Sata, Y., Shirai, M. & Sugimachi, M. 2010. Large conductance Ca^{2+}-activated K^+ channels inhibit vagal acetylcholine release at the rabbit sinoatrial node. *Auton Neurosci* **156**, 149–151.

Kawada, T., Shimizu, S., Li, M., Kamiya, A., Uemura, K., Sata, Y., Yamamoto, H. & Sugimachi, M. 2011. Contrasting effects of moderate vagal stimulation on heart rate and

Acta Physiologica © 2012 Scandinavian Physiological Society, doi: 10.1111/j.1748-1716.2012.02439.x

carotid sinus baroreflex-mediated sympathetic arterial pressure regulation in rats. *Life Sci* **89**, 498–503.

Kuusela, E., Raekallio, M., Anttila, M., Falck, I., Mölsä, S. & Vainio, O. 2000. Clinical effects and pharmacokinetics of medetomidine and its enantiomers in dogs. *J Vet Pharmacol Ther* **23**, 15–20.

Mancia, G., Grassi, G., Giannattasio, C. & Seravalle, G. 1999. Sympathetic activation in the pathogenesis of hypertension and progression of organ damage. *Hypertension* **34**, 724–728.

Masuda, Y. 2000. Role of the parasympathetic nervous system and interaction with the sympathetic nervous system in the early phase of hypertension. *J Cardiovasc Pharmacol* **36**(Suppl 2), S61–S64.

Matsuura, W., Sugimachi, M., Kawada, T., Sato, T., Shishido, T., Miyano, H., Nakahara, T., Ikeda, Y., Alexander, J. Jr & Sunagawa, K. 1997. Vagal stimulation decreases left ventricular contractility mainly through negative chronotropic effect. *Am J Physiol* **273**, H534–H539.

McDonough, P.M., Wetzel, G.T. & Brown, J.H. 1986. Further characterization of the presynaptic *alpha*-1 receptor modulating [^{3}H]ACh release from rat atria. *J Pharmacol Exp Ther* **238**, 612–617.

Minami, N. & Head, G.A. 2000. Cardiac vagal responsiveness during development in spontaneously hypertensive rats. *Auton Neurosci* **82**, 115–122.

Mitchell, J.H., Wallace, A.G. & Skinner, N.S. Jr 1963. Intrinsic effects of heart rate on left ventricular performance. *Am J Physiol* **205**, 41–48.

Nakayama, Y., Miyano, H., Shishido, T., Inagaki, M., Kawada, T., Sugimachi, M. & Sunagawa, K. 2001. Heart rate-independent vagal effect on end-systolic elastance of the canine left ventricle under various levels of sympathetic tone. *Circulation* **104**, 2277–2279.

Nalivaiko, E., Antunes, V.R. & Paton, J.F. 2010. Control of cardiac contractility in the rat working heart-brainstem preparation. *Exp Physiol* **95**, 107–119.

Nosaka, S. & Wang, S.C. 1972. Carotid sinus baroceptor functions in the spontaneously hypertensive rat. *Am J Physiol* **222**, 1079–1084.

Philbin, K.E., Bateman, R.J. & Mendelowitz, D. 2010. Clonidine, an α_2-receptor agonist, diminishes GABAergic neurotransmission to cardiac vagal neurons in the nucleus ambiguus. *Brain Res* **1347**, 65–70.

Robertson, H.A. & Leslie, R.A. 1985. Noradrenergic alpha$_2$ binding sites in vagal dorsal motor nucleus and nucleus tractus solitarius: autoradiographic localization. *Can J Physiol Pharmacol* **63**, 1190–1194.

Salgado, H.C., Barale, Á.R., Castania, J.A., Machado, B.H., Chapleau, M.W. & Fazan, R. Jr 2007. Baroreflex responses to electrical stimulation of aortic depressor nerve in conscious SHR. *Am J Physiol Heart Circ Physiol* **292**, H593–H600.

Shimizu, S., Akiyama, T., Kawada, T., Shishido, T., Yamazaki, T., Kamiya, A., Mizuno, M., Sano, S. & Sugimachi, M. 2009. In vivo direct monitoring of vagal acetylcholine release to the sinoatrial node. *Auton Neurosci* **148**, 44–49.

Shimizu, S., Akiyama, T., Kawada, T., Sata, Y., Mizuno, M., Kamiya, A., Shishido, T., Inagaki, M., Shirai, M., Sano, S. & Sugimachi, M. 2012. Medetomidine, an α_2-adrenergic agonist, activates cardiac vagal nerve through modulation of baroreflex control. *Circ J* **76**, 152–159.

Sinclair, M.D. 2003. A review of the physiological effects of α_2-agonists related to the clinical use of medetomidine in small animal practice. *Can Vet J* **44**, 885–897.

Snedecor, G.W. & Cochran, W.G. 1989. *Statistical Methods*. 8th edn, pp. 290–291. Iowa State, Iowa.

Tsunoda, M., Takezawa, K., Santa, T., Ina, Y., Nagashima, K., Ohmori, K., Kobayashi, S. & Imai, K. 2000. New approach for measurement of sympathetic nervous abnormality in conscious, spontaneously hypertensive rats. *Jpn J Pharmacol* **83**, 39–45.

34th Annual International Conference of the IEEE EMBS
San Diego, California USA, 28 August - 1 September, 2012

Consideration on Parameter Determination of a New Model Describing Dynamic Vagal Heart Rate Control in Rats

Toru Kawada, Kazunori Uemura, Shuji Shimizu, Atsunori Kamiya, Michael J Turner, Masaki Mizuno, Kenji Sunagawa, *Member, IEEE*, and Masaru Sugimachi, *Member, IEEE*

Abstract— **The dynamic characteristics of vagal heart rate control can be approximated by a first-order low-pass filter with pure dead time in rabbits. However, this model may not necessarily be the best approximation of the vagal transfer function of the heart rate control in rats, because a flatter portion exists in the gain plot above approximately 0.3 Hz. We developed a new model that includes a frequency-independent gain term to reproduce the flatter portion of the gain plot seen in the vagal transfer function in rats. The inclusion of the new term increased the coefficient of determination in an external validation of the linear regression relationship between measured and predicted heart rate responses to vagal stimulation, and made the slope of the regression line closer to unity. The parameters of mathematical transfer functions were determined in both the frequency and time domains. The frequency-domain fitting provided a set of parameters that was also able to reproduce the time-domain step response reasonably well. In contrast, the time-domain fitting provided a set of parameters that reproduced the frequency-domain transfer function only up to 0.2 Hz. Determination of proper model parameters was crucial for the development of a new model to describe the dynamic heart rate response to vagal stimulation in rats.**

I. Introduction

Dynamic heart rate control is important to adjust cardiac function to meet demands in daily activity. Both sympathetic and vagal systems are involved in the control of heart rate. Our previous study showed that dynamic characteristics of vagal heart rate control could be approximated by a first-order low-pass filter with pure dead time in rabbits [1]. However, a first-order low-pass filter with pure dead time is not necessarily the best approximation for the vagal transfer function of heart rate control in rats, because the transfer gain does not fall off smoothly above the corner frequency [2]. The gain plot exhibits a flatter portion in the frequency-domain around 0.3 Hz and above, which makes the transfer function deviate from a simple first-order low-pass filter with pure dead time. To describe the flatter portion in the gain plot, we propose a new model that includes a frequency-independent gain term in addition to the terms describing the low-pass nature of the dynamic heart rate control. The parameters of the proposed model were determined by the frequency-domain and time-domain methods.

Manuscript received March 12, 2012. This work was supported in part by Health and Labour Sciences Research Grants (H20-katsudo-Shitei-007, H21-nano-Ippan-005) from the Ministry of Health, Labour and Walfare of Japan, and a grant-in-aid for Scientific Research (23592319) from the Ministry of Education, Culture, Sports, Science and Technology of Japan.

T. Kawada, K. Uemura, S. Shimizu, A. Kamiya, M. J. Turner are with Department of Cardiovascular Dynamics, National Cerebral and Cardiovascular Center, Osaka 565-8565, Japan (corresponding author: T. Kawada, phone +81-6-6833-5012, fax: +81-6-6835-5403, e-mail: torukawa@ri.ncvc.go.jp).

M. Mizuno is with Department of Health Care Sciences, University of Texas Southwestern Medical Center, Dallas, TX, USA.

K. Sunagawa is with Department of Cardiovascular Medicine, Graduate School of Medical Sciences, Kyushu University, Fukuoka 812-8582, Japan.

II. Methods

A. Animal Preparation

The study was performed on 6 anesthetized Sprague-Dawley rats. Animals were cared for in strict accordance with the Guiding Principles for the Care and Use of Animals in the Field of Physiological Sciences, which has been approved by the Physiological Society of Japan. All experimental protocols were reviewed and approved by the Animal Subjects Committee at National Cerebral and Cardiovascular Center.

The rats were anesthetized with an intraperitoneal injection (2 ml/kg) of a mixture of urethane (250 mg/ml) and α-chloralose (40 mg/ml), and ventilated mechanically with oxygen-supplied room air. Supplemental anesthetic mixture was administered continuously. Arterial pressure was monitored through a catheter inserted into the right femoral artery. Heart rate was measured from body surface electrocardiogram using a cardiotachometer. In order to minimize systemic changes in sympathetic nerve activity, baroreceptor regions at bilateral carotid sinuses were isolated from the systemic circulation, and the intracarotid sinus pressure was maintained at 120 mmHg using a servo-controlled piston pump [3], [4], [5]. The aortic depressor nerves and vagi were sectioned bilaterally at the neck. A pair of stainless steel wire electrodes (Bioflex wire, AS633, Cooner Wire, CA, USA) was attached to the sectioned distal end of the right vagus for electrical stimulation.

To estimate dynamic characteristics of the vagal heart rate control, the right vagus was stimulated for 15 min according to a binary white noise signal. The command signal was assigned to either 0 or 20 Hz every 0.5 s. As a result, the input power spectrum was relatively constant up to 1 Hz.

B. Data Analysis

Experimental data were stored at 1000 Hz using a 16-bit analog-to-digital converter. To avoid the possibility that the initial transition from zero stimulation to the binary white noise stimulation biasing the transfer function estimation, the data were analyzed starting 2 min after the initiation of

stimulation. Input-output data pairs were resampled at 10 Hz, and partitioned into 10 half-overlapping segments consisting of 1024 data points each. In each segment, the linear trend was subtracted and a Hanning window was applied. Frequency spectra of the input [$X(f)$] and the output [$Y(f)$] were obtained via the fast Fourier transform. The input power [$S_{XX}(f)$], output power [$S_{YY}(f)$], and the cross spectra between the input and output [$S_{YX}(f)$] were calculated over the 10 segments. Finally, the transfer function from vagal stimulation to the heart rate response was calculated using the following equation [6]:

$$H(f) = \frac{S_{YX}(f)}{S_{XX}(f)}$$

To quantify the linear dependence of the heart rate response to the vagal stimulation, the magnitude squared coherence function was calculated using the following equation:

$$Coh(f) = \frac{|S_{YX}(f)|^2}{S_{XX}(f) S_{YY}(f)}$$

To help intuitive understanding of the system behavior, the system step response was calculated from a time integral of the system impulse response which was derived from the inverse Fourier transform of the transfer function. Hereafter in this paper, this step response is referred to as an "nonparametric" step response.

In the original model (Model A) we used a first-order low-pass filter with pure dead time as described below [1].

$$M_A(f) = \frac{K}{1 + \frac{f}{f_C} j} \exp(-2\pi f L j)$$

where K is the steady-state gain, f_C is the corner frequency (in Hz), and L is the pure dead time (in s). j represents the imaginary units. The step response corresponding to Model A is as follows.

$$\begin{cases} S_A(t) = 0 & (t < L) \\ S_A(t) = K\left[1 - \exp\left(-\frac{t-L}{\tau}\right)\right] & (L \le t) \end{cases}$$

$$\tau = \frac{1}{2\pi f_C}$$

Our newly proposed model (Model B) is a combination of the first-order low-pass filter and a frequency-independent gain term as follows.

$$M_B(f) = K\left(\frac{1-R}{1 + \frac{f}{f_C} j} + R\right) \exp(-2\pi f L j)$$

where R ($0 \le R < 1$) represents the fraction of the frequency-independent gain relative to the steady-state gain. Although other models could be possible, Model B is thought to be most convenient because it provides the steady-state gain by K as in Model A. When $R > 0$ Model B can be rewritten as:

$$M_B(f) = K\left(\frac{1 + \frac{f}{f_R} j}{1 + \frac{f}{f_C} j}\right) \exp(-2\pi f L j)$$

where $f_R = f_C/R$. Because R is defined as a value less than unity, f_R is greater than f_C. The step response corresponding to Model B is as follows.

$$\begin{cases} S_B(t) = 0 & (t < L) \\ S_B(t) = K\left[1 - (1-R)\exp\left(-\frac{t-L}{\tau}\right)\right] & (L \le t) \end{cases}$$

The model parameters were estimated in both the frequency domain and the time domain. In the time-domain fitting, the sum of squared errors between the model step response and the nonparametric step response was minimized using a nonlinear iterative least square fitting. In the frequency-domain fitting, the following error function was employed.

$$E = \sum_{k=1}^{N} \frac{[\log(H(f_k)) - \log(M(f_k))]^2}{k} = \sum_{k=1}^{N} \frac{1}{k}\left[\log\left(\frac{H(f_k)}{M(f_k)}\right)\right]^2$$

$$f_k = f_0 \times k$$

where f_0 is the fundamental frequency of the Fourier transform, k is an index of the frequency, and f_k is the k-th frequency. N represents the frequency index up to which the error was considered. In the present study, N was set at 120, which corresponded to 1.17 Hz. $H(f)$ and $M(f)$, which are both complex values, represent the experimental and model transfer functions, respectively. The error function took the logarithmic representation of the system dynamic characteristics on the Bode plot into account. In this context, there was no difference whether the natural or common logarithm were used, as the task of fitting was to find a set of parameters to minimize the error function.

After the model parameters were estimated, the dynamic heart rate response to vagal stimulation was predicted from the convolution of the command signal with the impulse response derived from the model transfer function. The regression analysis for the measured versus the predicted heart rate response was performed using a data set that was obtained externally to the segments used for the estimation of the transfer function (i.e., external validation). The output signal of 2048 points was predicted.

III. Results and Discussion

Figure 1 illustrates a typical example of the transfer function from vagal stimulation to the heart rate response obtained in one animal (solid lines). In the gain plot, the transfer gain decreased as the frequency increased above 0.02 Hz, suggesting low-pass characteristics of the heart rate response to vagal stimulation. The transfer gain, however, did not fall off smoothly beyond 0.3 Hz, creating a flatter portion in the higher frequency range. In the phase plot, the phase was close to $-\pi$ radians at the lowest frequency, and delayed with increasing frequency. These phase characteristics suggest that the heart rate response to vagal stimulation should be negative

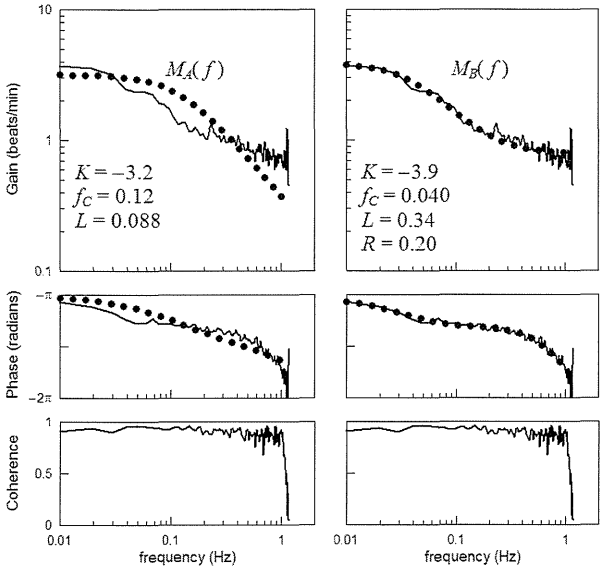

Figure 1. Transfer function from vagal stimulation to the heart rate response (solid lines) and model tranfer functions (circled lines).

at steady state. The coherence was high up to 1 Hz, suggesting that the heart rate response can mostly be described by linear dynamics in the present experimental settings. Therefore, the flatter portion observed in the gain plot is not likely the result of a reduction in the accuracy of the transfer function estimation in the higher frequency range.

The circles in the left panels of Figure 1 represent the transfer function of Model A with its parameters determined by the frequency-domain fitting. There was a significant deviation between Model A and experimental transfer functions such that the steady-state gain was estimated to be lower in Model A compared with the experimental transfer function. The corner frequency was estimated to be higher in Model A than in the experimental transfer function. Therefore, frequency-domain parameter determination does not work well when a given model does not have the degree of freedom

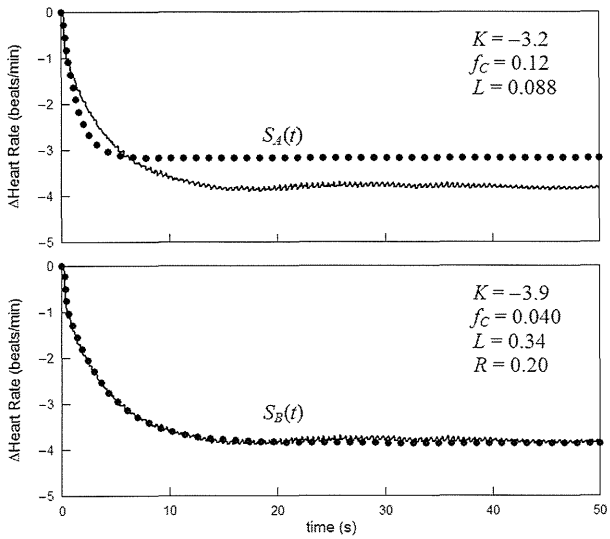

Figure 2. Step response of the heart rate response to vagal stimulation (solid lines) and model step responses based on the frequency-domain parameter determination (circles).

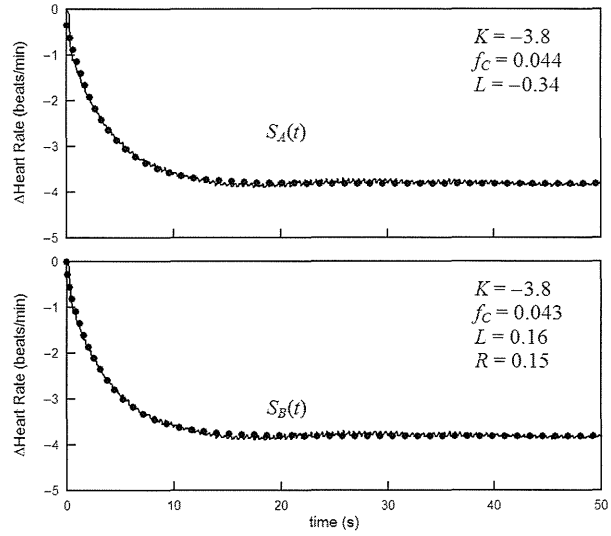

Figure 3. Step response of the heart rate response to vagal stimulation (solid lines) and model step responses based on the time-domain parameter determination (circled lines).

to reproduce an experimental transfer function.

The circles in the right panels of Figure 1 indicate the transfer function of Model B with its parameters determined by the frequency-domain fitting. The model transfer function reproduced the characteristics of the experimental transfer function reasonably well in the frequency range from 0.01 to 1 Hz.

Figure 2 depicts the step responses corresponding to the transfer functions shown in Figure 1. In the top panel, the step response of Model A underestimated the steady-state response relative to that of the nonparametric step response. The time constant was estimated to be shorter, which is equivalent to the higher corner frequency in the frequency domain. In the bottom panel, the step response of Model B reproduced the nonparametric step response well.

While Model A did not reproduce the experimental step response well when parameters were determined in the frequency domain, both models A and B were able to mimic the nonparametric step response when parameters were determined in the time domain (Figure 3). However, the lag time was estimated to be negative in Model A, which is physically unrealizable.

Figure 4 illustrates the transfer function from vagal stimulation to the heart rate response (solid lines) and the model transfer functions (circles) with their parameters determined in the time domain to minimize the error between the model and nonparametric step responses. While both models A and B reproduced the experimental transfer function up to 0.2 Hz, the model transfer functions deviated from the experimental transfer function in the frequency range above 0.2 Hz. Therefore, even though the model step response appeared to mimic the nonparametric step response, there can be a significant deviation in the higher frequency range when examined in the frequency domain. In the present case, because the fraction of the frequency-independent gain relative to the steady-state gain was approximately 0.2, the

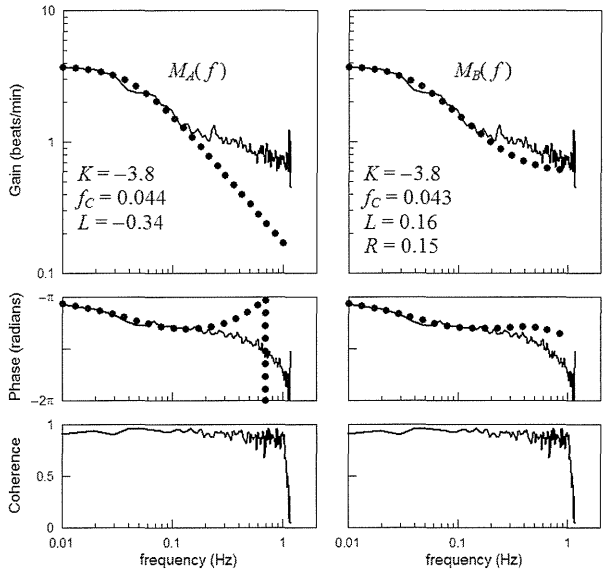

Figure 4. Transfer function from vagal stimulation to the heart rate response (solid lines) and model tranfer functions based on the time-domain parameter determination (circles).

majority of the step response could be described by the parameters relating to the first-order low-pass filter.

Figure 5 illustrates the actually measured dynamic heart rate response to vagal stimulation versus the heart rate responses predicted by Model A (top panel) and Model B (bottom panel). Close inspection of the figure indicates that Model A was not able to reproduce sharp rises in the heart rate response (marked with asterisks) in contrast with Model B. The scatter plots of the measured versus the predicted heart rate are shown in the right panels of Figure 5. The coefficient of determination was higher for the prediction when using Model B compared with Model A.

The regression analysis on data obtained from 6 rats shows that the slope of the regression line was 0.81±0.05 for the heart rate prediction by Model A, and was 0.94±0.03 for the heart rate prediction by Model B. In all six animals, the coefficient of determination was higher in the prediction by Model B (ranged from 0.71 to 0.91) than in the prediction by

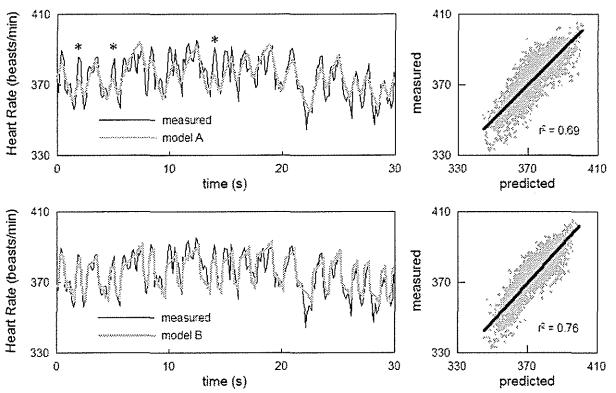

Figure 5. Measured (solid lines) and model-predicted (gray lines) of the heart rate response to vagal stimulation. The top panels are the results ofmodel A and the bottom panels are the results of model B. The coefficient of determination was higher for the prediction by model B.

Model A (ranged 0.56 to 0.90). While the increment of the number of model parameters itself should increase the coefficient of determination, because the regression analysis was performed on a data set that was not used for the estimation of the transfer function (i.e., external validation), it may be fair to say that Model B provided a better prediction of the heart rate response compared with Model A.

There are several limitations to the present study. First, the heart rate of the anesthetized rats was 300–400 beats/min (5–6.7 Hz), which indicates that the Nyquist frequency may be as low as 2.5 Hz for the heart rate data. The heart rate signal cannot reproduce frequency components above this frequency. Although we included a frequency-independent gain term to explain the flatter portion in the gain plot observed in the experimental transfer function, there is an inherent upper frequency limit to the heart rate control, above which the model is likely to deviate from the experimental transfer function. Second, the frequency-independent gain term suggests the presence of a rapid responding system parallel to the low-pass system in the vagal heart rate control in rats. While the inclusion of the frequency-independent gain term improved the prediction of the dynamic heart rate response to vagal stimulation, the mechanisms for the rapid responding system are largely unknown. Further studies are required to identify the mechanisms and the physiological significance for the rapid responding system observed in rats but not in rabbits.

REFERENCES

[1] T. Kawada, Y. Ikeda, M. Sugimachi, T. Shishido, O. Kawaguchi, T. Yamazaki, et al. "Bidirectional augmentation of heart rate regulation by autonomic nervous system in rabbits," *Am. J. Physiol. Heart Circ. Physiol.*, vol. 271, pp. H288-H295, 1996.

[2] M, Mizuno, T. Kawada, A. Kamiya, T. Miyamoto, S. Shimizu, T. Shishido, et al. "Dynamic characteristics of heart rate control by the autonomic nervous system in rats," *Exp. Physiol.*, vol. 95, pp. 919-925, 2010.

[3] A. A. Shoukas, C. A. Callahan, J. M. Lash, E. B. Haase. "New technique to completely isolate carotid sinus baroreceptor regions in rats," *Am. J. Physiol. Heart Circ. Physiol.*, vol. 260, pp. H300-H303, 1991.

[4] T. Sato, T. Kawada, H. Miyano, T. Shishido, M. Inagaki, R. Yoshimura, et al. "New simple methods for isolating baroreceptor regions of carotid sinus and aortic depressor nerves in rats," *Am. J. Physiol. Heart Circ. Physiol.*, vol. 276, pp. H326-H332, 1999.

[5] T. Kawada, M. Li, A. Kamiya, S. Shimizu, K. Uemura, H. Yamamoto, et al. "Open-loop dynamic and static characteristics of the carotid sinus baroreflex in rats with chronic heart failure after myocardial infarction," *J. Physiol. Sci.*, vol. 60, pp. 283-298, 2010.

[6] P. Z. Marmarelis, V. Z. Marmarelis. Analysis of Physiological Systems. The White-Noise Approach. New York and London: Plenum Press, 1978, pp. 131-178.

Cardiovasc Drugs Ther (2012) 26:217–226
DOI 10.1007/s10557-012-6381-5

H_2 Mediates Cardioprotection Via Involvements of K_{ATP} Channels and Permeability Transition Pores of Mitochondria in Dogs

Akemi Yoshida · Hiroshi Asanuma · Hideyuki Sasaki · Shoji Sanada · Satoru Yamazaki · Yoshihiro Asano · Yoshiro Shinozaki · Hidezo Mori · Akito Shimouchi · Motoaki Sano · Masanori Asakura · Tetsuo Minamino · Seiji Takashima · Masaru Sugimachi · Naoki Mochizuki · Masafumi Kitakaze

Published online: 17 April 2012

Abstract
Purpose Inhalation of hydrogen (H_2) gas has been shown to limit infarct size following ischemia-reperfusion injury in rat hearts. However, H_2 gas-induced cardioprotection has not been tested in large animals and the precise cellular mechanism of protection has not been elucidated. We investigated whether opening of mitochondrial ATP-sensitive K+ channels (mK_{ATP}) and subsequent inhibition of mitochondrial permeability transition pores (mPTP) mediates the infarct size-limiting effect of H_2 gas in canine hearts.
Methods The left anterior descending coronary artery of beagle dogs was occluded for 90 min followed by reperfusion for 6 h. Either 1.3% H_2 or control gas was inhaled from 10 min prior to start of reperfusion until 1 h of reperfusion, in the presence or absence of either 5-hydroxydecanoate (5-HD; a selective mK_{ATP} blocker), or atractyloside (Atr; a mPTP opener).
Results Systemic hemodynamic parameters did not differ among the groups. Nevertheless, H_2 gas inhalation reduced infarct size normalized by risk area (20.6±2.8% vs. control gas 44.0±2.0%; $p<0.001$), and administration of either 5-HD or Atr abolished the infarct size-limiting effect of H_2 gas (42.0±2.2% with 5-HD and 45.1±2.7% with Atr; both $p<0.001$ vs. H_2 group). Neither Atr nor 5-HD affected infarct size per se. Among all groups, NAD content and the number of apoptotic and 8-OHdG positive cells was not significantly different, indicating that the cardioprotection

A. Yoshida · H. Sasaki · S. Yamazaki · M. Asakura · M. Kitakaze (✉)
Department of Cardiovascular Medicine, National Cerebral and Cardiovascular Center, Suita 565-8565, Osaka, Japan
e-mail: kitakaze@zf6.so-net.ne.jp

H. Asanuma
Department of Cardiovascular Science and Technology, Kyoto Prefectural University of Medicine, Suita 565-8565, Osaka, Japan

A. Yoshida · N. Mochizuki
Department of Structural Analysis, National Cerebral and Cardiovascular Research Center, Suita, Japan

S. Sanada · Y. Asano · T. Minamino · S. Takashima
Department of Cardiovascular Medicine, Osaka University Graduate School of Medicine, Suita, Japan

Y. Shinozaki · H. Mori
Department of Physiological Science, Tokai University Graduate School of Medicine, Isehara, Japan

A. Shimouchi
Department of Cardiac Physiology, National Cerebral and Cardiovascular Research Center, Suita, Japan

M. Sano
Department of Cardiology, Keio University School of Medicine, Tokyo, Japan

M. Sugimachi
Department of Cardiovascular Dynamics, Research Institute, National Cerebral and Cardiovascular Center, Suita, Japan

afforded by H_2 was not due to anti-oxidative actions or effects on the NADH dehydrogenase pathway.
Conclusions Inhalation of H_2 gas reduces infarct size in canine hearts via opening of mitochondrial K_{ATP} channels followed by inhibition of mPTP. H_2 gas may provide an effective adjunct strategy in patients with acute myocardial infarction receiving reperfusion therapy.

Key words Hydrogen gas · Reperfusion injury · Myocardial infarction · Mitochondrial K_{ATP} channel · Mitochondrial permeability transition pore

Introduction

Myocardial infarction (MI) is a leading cause of death worldwide, and reduction of infarct size is an important therapeutic goal for patients with acute MI (AMI). The prognosis of AMI has been improved dramatically due to the development of both catheterization techniques and reperfusion therapy by coronary mechanical methods or pharmacological intervention. However, strategies to limit reperfusion injury and thus infarct size have not been well applied in clinical settings [1, 2]. We reported that carperitide limited infarct size in a large scale clinical trial [3]; however, infarct size was reduced by only 14.7%, and the discovery of other therapeutics to limit infarct size may be clinically useful. Interestingly, hydrogen (H_2) has been reported to provide therapeutic benefit for many diseases related to oxidative stress, including cardiovascular disease. There is some evidence that inhalation of H_2 gas limits myocardial infarct size in rats [4, 5]. However, since heart physiology differs significantly in small animals relative to large animals and humans, it cannot be assumed that H_2 would limit infarct size in large animals and humans. Furthermore, the cellular mechanisms underlying H_2-mediated cardioprotection have not been clarified.

Recent accumulated evidence regarding cardioprotection afforded by ischemic pre- or post-conditioning has culminated in the idea that opening of mitochondrial ATP-sensitive K^+ channels (mK_{ATP}) followed by inhibition of mitochondrial permeability transition pores (mPTP) plays a central role in limiting infarct size [6–8]. Indeed, Piot et al. [9] found that administration of the mPTP inhibitor, cyclosporine, at the time of reperfusion limited the size of myocardial infarction in patients with AMI. Ohsawa et al. [10] demonstrated that H_2 has the potential to serve as an antioxidant in preventive and therapeutic applications. Oxygen-derived free radicals are generated inside and outside of cells, and H_2 gas can eliminate hydoxyradical and peroxynitrate because it can penetrate biomembranes and diffuse into the cytosol, mitochondria, and nuclei. If this is the case, H_2 gas may protect mK_{ATP} against ischemic injury, or may directly activate mK_{ATP} followed by the inhibition of mPTP.

Thus, we tested the hypothesis that H_2 gas may reduce reperfusion injury and limit infarct size via the activation of mK_{ATP} and the inhibition of mPTP.

Methods

Animal model and instrumentation

Fifty nine beagle dogs (Oriental Yeast Co., Ltd, Tokyo, Japan) weighing 9 to 10 kg were per-anesthetized with sodium pentobarbital (25 mg/kg iv). All dogs were rapidly intubated and anesthetized with analgesic anesthetics. The control or H_2 gas tank was connected to the respirator 10 min before reperfusion. After baseline hemodynamic assessment, thoracotomy was performed, and the left anterior descending coronary artery (LAD) was ligated just distal to the first diagonal branch. The left carotid artery was catheterized to monitor both aortic blood pressure and heart rate. At the end of each study, animals were euthanized with administration of a high dose of sodium pentobarbital. All procedures were performed in conformity with the Guide for the Care and Use of Laboratory Animals (NIH publication no. 85-23, 1996 revision).

Composition of gas mixture

Gas tanks were obtained from TAIYO NIPPON SANSO Corporation (Osaka, Japan). The control gas tanks were composed of 70% N_2 and 30% O_2. The H_2 gas tanks were composed of 1.3% H_2, 68.7% N_2, and 30% O_2. The H_2 gas concentration was set at 1.3% because higher concentrations create the possibility of explosion. Previous studies showed that 0.5%–4.0% H_2 limited infarct size in rat hearts in vivo, at a flow rate of 1 L/min.

Experimental protocols

After the randomization to either H_2 gas (n=18) or control gas (n=18), the LAD of the beagle was occluded for 90 min followed by reperfusion for 6 h. Either H_2 gas or control gas was inhaled (3.36 L/min) 10 min prior to reperfusion until 1 h of reperfusion. In addition, we intravenously administered either 5-hydroxydecanoate (5-HD, Sigma; 10 mg/kg i.v.), or atractyloside (Atr, Sigma; 2.5 mg/kg i.v.), for 5 min before gas inhalation [H_2 gas with 5-HD (n=6) or Atr (n=6) and control gas with 5-HD (n=6) or Atr (n=6)]. In all groups, infarct size was assessed after 6 h of reperfusion. We also investigated apoptosis in the myocardium adjacent to the infarct area using TUNEL staining. In addition, we counted the incidence of lethal arrhythmia, defined as more than 15 consecutive premature ventricular contractions (VPC) or ventricular fibrillation (Vf) from 10 min before reperfusion to 60 min after the onset of reperfusion.

Measurement of infarct size and myocardial collateral blood flow

We measured both area at risk and infarct area 6 h after the onset of reperfusion as described previously [11]. These parameters were evaluated by Evans blue and triphenyltetrazolium chloride (TTC) staining, respectively. Infarct size was calculated as [infarct area/area at risk] × 100(%).

Regional myocardial blood flow was determined by the microsphere technique. Non-radioactive microspheres (Sekisui Plastic Co., Ltd., Tokyo, Japan) are made of inert plastic labeled with niobium (Nb) and bromine (Br) as described in detail in previous study [12]. Microspheres were suspended in isotonic saline with 0.01% Tween80 to prevent aggregation. The microspheres were ultrasonicated for 5 min followed by 5 min of vortexing immediately before injection. Approximately 1 mL of the microsphere suspension ($2–4\times10^5$ spheres) was injected into the left atrium at 80 min after the start of coronary occlusion.

The X-ray fluorescence of stable heavy elements was measured by a wavelength dispersive spectrometer (PW 1480, PHILLIPS Co., Ltd.). The specifications of this X-ray fluorescence spectrometer have been described previously [12]. In brief, when the microspheres are irradiated by the primary X-ray beam, the electrons fall back to a lower orbit and emit measurable energy. The energy level of the X-ray fluorescence depends on the characteristics of each element. Therefore, it was possible to quantify the X-ray fluorescence of several differently labeled microspheres in the mixture. Regional myocardial collateral blood flow was calculated according to the following formula: time flow = (tissue count) × (reference flow)/(reference count), and was expressed in mL/g wet weight/min.

Terminal Deoxynucleotidyl transferase-mediated dUTP nick-end labeling (TUNEL)

The myocardial tissue samples were taken from the border zone of dogs in the control, H_2, control+5-HD, H_2+5-HD, control+Atr and H_2+Atr groups (n=3 each). The border zone was chosen as the region within 4 mm from the infarct zone. These were fixed in 10% buffered formalin, embedded in paraffin, and serially sectioned in the frontal plane at 5-μm thickness. To assess myocardial apoptosis, analysis by TUNEL method was performed according to the protocol supplied with the in situ apoptosis detection kit, the Apop Tag Peroxidase In Situ Apoptosis Detection Kit (S7100, MILLIPORE). The sections were then shortly counterstained with hematoxylin and eosin to visualize the cells. TUNEL-positive cell nuclei and total cell nuclei stained metylgreen were counted in 7–10 random high-power fields (×200). The amount of TUNEL-positive cells was expressed as a percentage of the total amount of cells (n=1,500).

Immunohistochemistry for either 8-OHdG or NAD+ of the Reperfused myocardium

The myocardial tissue samples were taken from the border zone between ischemic and non-ischemic areas in the control, H_2, H_2+5-HD, H_2+Atr, control+5-HD and control+Atr groups (n=3 each). After 90 min of ischemia followed by 6 h of reperfusion, hearts were excised and the myocardial tissue samples were taken from the border zone. The border zone was chosen as the region within 4 mm from the infarct zone. These were fixed in 10% buffered formalin, embedded in paraffin, and serially sectioned in the frontal plane at 5-μm thickness. The paraffin sections were deparaffinized in xylene, rehydrated using various grades of ethanol, and pretreated with 10 mM citric acid for 40 min at 95°C. For immunostaining, sections stained with anti-8OH-dG (MOG-020P; Japan Institute for the Control of Aging; 1:100) antibodies overnight at 4°C. Secondary antibodies conjugated Simple Stain Rat (MAX-PO MULTI 414191, NICHIREI Bioscience inc. Japan; undiluted) were applied for 30 min at room temperature. The sections were then shortly counterstained with hematoxylin and eosin to visualize the cells. Four slides were randomly examined using a defined rectangular field area with magnification (×40). The data were represented as the number of 8OH-dG positive cells per field.

Since mPTP may be opened via oygen-drived free radicals via the NADPH oxidase, we also investigated the myocardial NAD+ contents as well. We used 18 dogs for NAD assessment in the control, H_2, H_2+5-HD, H_2+Atr, control+5-HD and control+Atr groups (n=3 each). The myocardial tissue in the border zone was quickly placed into liquid nitrogen and stored at −80°C. For the measurement of NAD+, 40 mg of border zone tissue was homogenized. An equal amount of protein from the homogenized tissue of each group was used for the NAD+/NADH Colorimetric assay kit (Cat# CY-1253; Cyclex Co., Ltd).

Exclusion criteria

To ensure that all animals used in the present study were healthy and had been exposed to a similar extent of ischemia, the following standards were employed for the exclusion of unsatisfactory dogs: (1) subendocardial collateral blood flow greater than 15 mL/100 g/min; (2) heart rate greater than 170 beats/min; and (3) more than two consecutive attempts required to terminate ventricular fibrillation (Vf) using low-energy DC pulses applied directly to the heart.

Statistical analysis

Statistical analysis was performed using two-way repeated measures analysis of variance (ANOVA) when data were

compared over the time course of the change between groups. Analysis of covariance between regional collateral flow in the inner half of the left ventricular wall and infarct size was described previously [11]. Other data were compared using one-way fractional analysis of variance. If statistical significance was found for a group, time effect, or group-by-time interaction, further comparisons were made with paired t tests between all possible pairs of the five groups at individual time points. Results were expressed as means ± SEM, with $p<0.05$ considered statistically significant.

Results

Among the 59 dogs, 23 were excluded due to Vf or excessive myocardial collateral blood flow (>15 mL/100 g/min). The remaining 36 dogs completed the protocols satisfactorily and were included in the data analysis. None of the pharmacological interventions such as H_2 gas, control gas, 5-HD, or Atr, altered systemic blood pressure or heart rate during the experimental protocols (Table 1).

Inhalation of H_2 gas just prior to reperfusion following 90 min of ischemia reduced infarct size normalized by risk area (20.6±2.8% vs. 44.0±2.0%; $p<0.001$) (Fig. 1). Intriguingly, the administration of either 5-HD or atractyloside (Atr) blunted the H_2 gas induced limiting effect on infarct size (42.0 ±2.2% in 5-HD vs. 45.1±2.7% in Atr; $p<0.001$ and $p<0.001$ vs. H_2 gas group). Neither 5-HD nor atractyloside per se affected infarct size. There were no differences in either risk area or collateral flow during the ischemic period among the groups (Fig. 2). Figure 3 shows the regression plots of the area at risk vs. collateral flow. Inhalation of H_2 gas mediated the substantial cardioprotection irrespective of collateral flow, which was again blunted by either 5-HD or atractyloside.

On the other hand, we observed apoptosis using TUNEL staining in the myocardium in each group; there were no differences in the extent of apoptosis in the groups (36.0± 1.8, 26.5±6.9, 33.0±1.4, 35.6±1.5, 35.0±1.3 and 35.7±1.4% in the control group, the H_2 gas group, the H_2 gas with 5HD group, the H_2 gas with Atr group, the control gas with 5HD group, and the control gas with Atr group, respectively).

We observed the incidence of lethal arrhythmia throughout the experiments in all groups from 10 min before reperfusion to 60 min after the onset of reperfusion (Table 2). The presence of either Vf or VPC longer than 15 consecutive beats was defined as lethal arrhythmia in this study. The incidence of lethal arrhythmia in the reperfusion period tended to decrease by H_2 gas although there were no significant differences. This tendency was blunted by either 5-HD or Atr. These data indicate that H_2 gas may affect the incidence of fatal ventricular arrhythmias during the reperfusion period, but it is unknown whether this effect is attributable to a potential primary anti-arrhythmic effect of H_2 gas or merely secondary to the infarct size-limiting effects of H_2 gas.

The number of 8-OHdG (a biomarker of oxidative stress) positive cells, tended to decrease in H_2 group relative to the other groups, however there was no significant difference (Fig. 4). We also observed no relation between the number

Table 1 Effect of H_2 gas on systemic hemodynamic parameters

Groups	Baseline	Isc-60	Isc-90	Rep-60	Rep-120	Rep-180	Rep-240	Rep-300	Rep-240
Mean blood pressure (mmHg)									
Control gas	101±2	103±2	104±2	98±2	102±2	101±3	103±3	99±3	100±2
H_2 gas	105±4	97±2	98±3	96±3	100±2	101±3	99±2	101±2	103±1
H_2 gas + 5HD	105±2	105±2	106±1	95±3	98±3	101±3	103±1	102±0	100±4
H_2 gas + Atr	98±3	98±3	102±3	98±1	100±1	101±1	102±1	102±2	103±1
Control gas + 5HD	104±2	101±2	101±1	102±2	103±2	101±3	103±2	98±3	100±4
Control gas + Atr	102±1	102±4	100±2	96±1	103±2	100±3	103±2	104±2	102±1
Heart rate (beats/min)									
Control gas	136±3	138±2	137±2	132±2	131±1	135±3	135±4	133±4	133±4
H_2 gas	139±3	138±3	140±4	133±3	134±4	134±5	134±4	134±5	132±4
H_2 gas + 5HD	135±3	130±3	129±4	129±3	129±4	130±3	129±4	129±4	130±3
H_2 gas + Atr	134±2	135±4	130±4	129±3	129±2	129±3	129±2	128±3	129±3
Control gas + 5HD	134±4	135±3	135±3	135±2	129±3	131±5	132±5	130±5	129±5
Control gas + Atr	137±2	137±2	135±3	136±2	137±3	135±4	135±2	135±3	136±2

Values are expressed as mean ± SEM. Isc-60 and Isc-90 show 60 and 90 min after the onset of myocardial ischemia, respectively. Rep-60, Rep-120, Rep-180, Rep-240, Rep-300 and Rep-360 show 60, 120, 180, 240, 300 and 360 min after the onset of reperfusion, respectively. There were no significant changes of theses parameters among the six groups

5HD = 5-hydroxydecanoate; Atr = Atractyloside

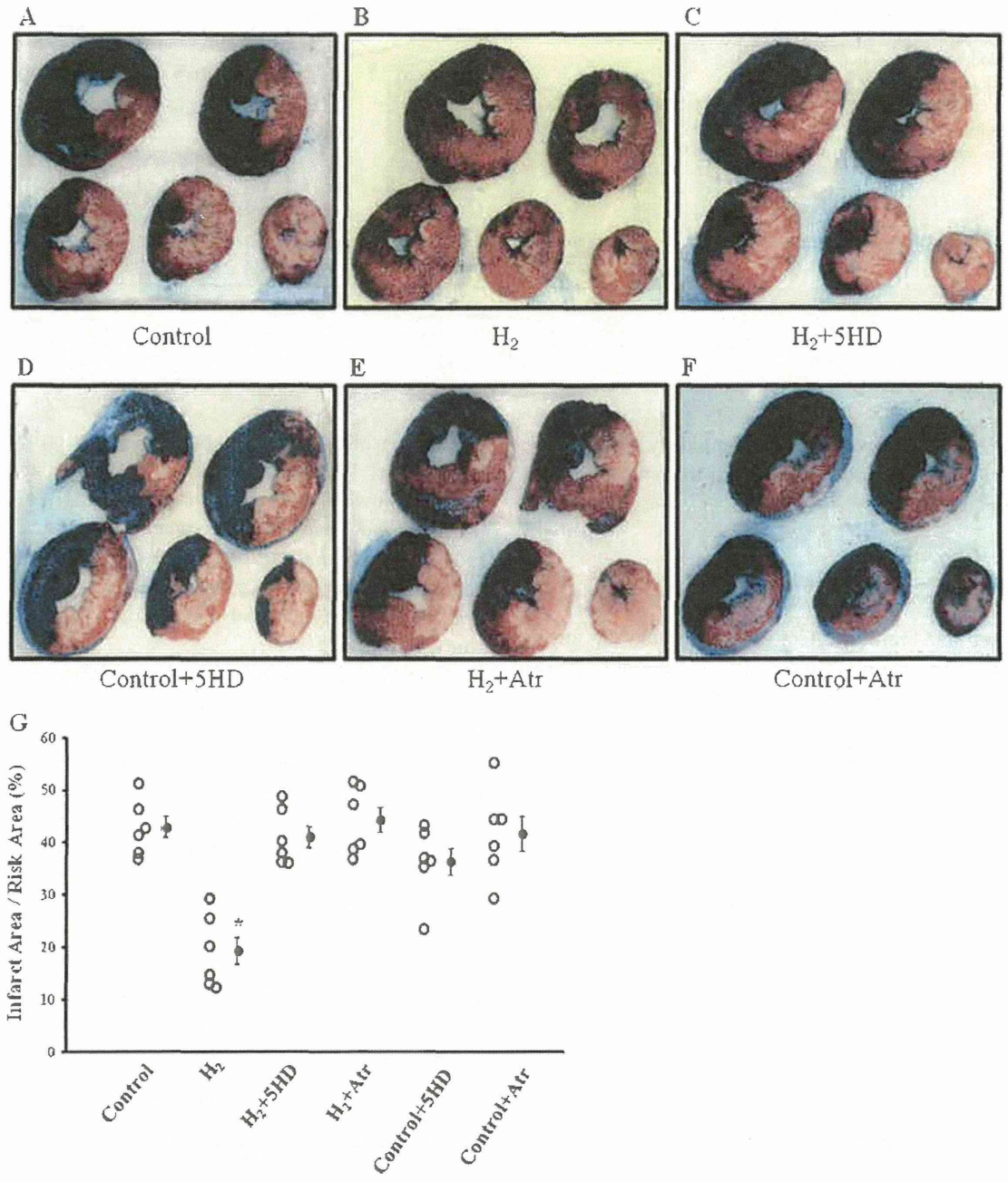

Fig. 1 Effect of H_2 Gas on Myocardial Infarct Size. Values are expressed as mean ± SEM (error bars). Representative photos following both Evans Blue and triphenyltetrazolium chloride staining are shown in the control gas (**A**), H_2 gas (**B**), H_2 gas with 5HD (**C**), H_2 gas with Atr (**D**), control gas with 5HD (**E**), and the control gas with Atr groups (**F**) respectively. **G** Myocardial infarct size quantification as a percentage of the area at risk in groups tested. Inhalation of hydrogen gas reduced infarct size. 5HD and Atr abolished this cardioprotective effect. *$p<0.0001$ vs. control group. 5HD = 5-hydroxydecanoate; Atr = atractyloside

of 8-OHdG positive cells and infarct size. We next investigated myocardial NAD+ levels and observed a not significant tendency towards increased NAD+ levels in the H_2 group, suggesting that the inhibition of mPTP caused by the opening of mK_{ATP} may not be attributable to oxygen-derived free radicals produced through NADH dehydrogenase (Fig. 5).

Discussion

The present study provides a novel finding that inhalation of H_2 gas mediates infarct size-limiting effects but not cellular apoptosis-limiting effects in the canine heart large animal model, and that H_2 gas-mediated cardioprotection is mainly attributable to the opening of mK_{ATP} followed by inhibition

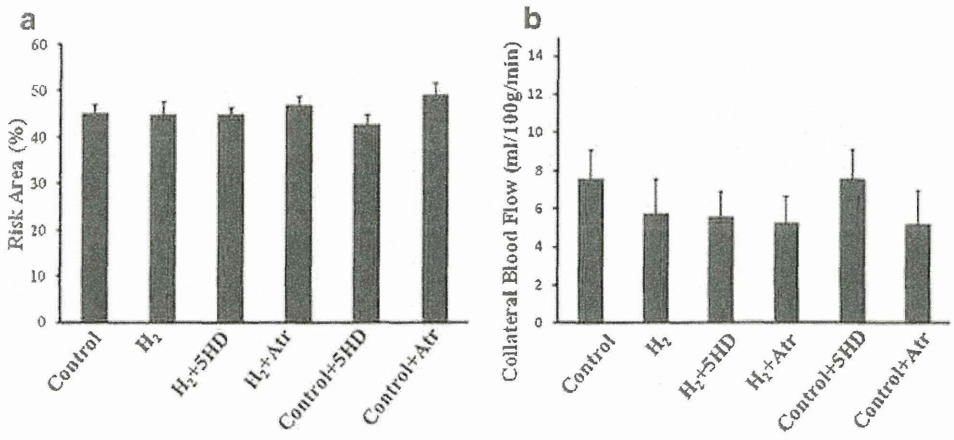

Fig. 2 Risk Area and Collateral Flow. Risk area (**a**) and collateral blood flow (**b**). There were no differences in either risk area or collateral blood flow in all groups. Values are expressed as mean ± SEM (error bars)

of mPTP, although we could not completely exclude the involvements of H_2 gas-mediated anti-oxidant effects on the present results.

Factors that affect infarct size during inhalation of H_2 gas

The infarct size-limiting effect of H_2 gas may be attributable to changes in systemic hemodynamics and/or collateral flow, because these two factors are critical in determining infarct size. However, when H_2 gas was inhaled, systemic blood pressure, heart rate, and collateral flow were unchanged among the groups. Therefore, H_2 gas-induced cardioprotection is not mediated by hemodynamic or collateral flow changes secondary to the inhalation of H_2 gas. Myocardial contractility is another determinant of infarct size, since increases in myocardial contractility may increase infarct size; indeed, beta blockers, which reduce myocardial contractility, reduce infarct size. However, Hayashida et al. [5] and Sun et al. [4] showed that either H_2 gas or H_2-rich saline provokes no changes in myocardial contractility as a index of maximal dP/dt, suggesting that myocardial contractility is not altered by H_2 gas, although we did not measure myocardial contractility in the present study.

We have shown that H_2 gas limits infarct size in large animals, which may be translated to human use. In rats, heart rate and maximal dP/dt are around 400/min, and 8,000 mmHg/sec, respectively [5]. However, in the anesthetized dog, these parameters are around 130/min and 4,000 mmHg/sec, respectively [13, 14]. Therefore, the fact that H_2 gas limits infarct size in rat hearts does not necessarily indicate that this will be the case in large animals. We found cardioprotective effects of H_2 gas in canine hearts, indicating that potent cardioprotection by H_2 gas or H_2-rich saline may be the case for possible human use. However, in our large animal model, apoptosis was not prevented by H_2 gas, which is different from results seen by Sun et al. [4]. We

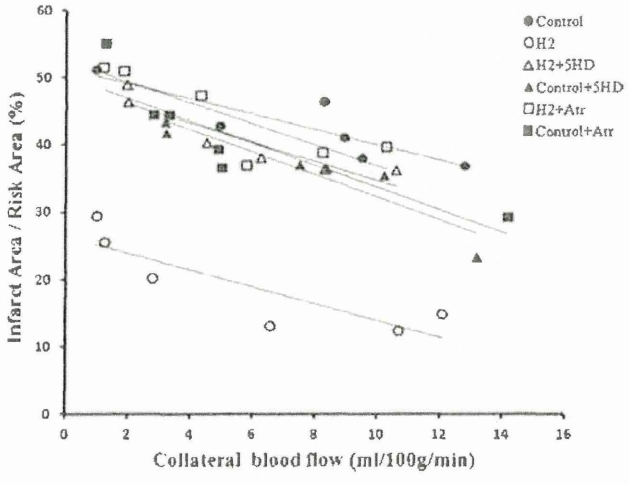

Fig. 3 Plot of infarct size expressed as a percentage of the risk area and regional collateral flow during ischemia. The abbreviations are same as in Fig. 1 There are inverse relations between normalized infarct area and collateral flow, and a significant difference ($P<0.05$) is seen in the H_2 gas group compared with the control group

Table 2 Incidence of lethal arrhythmia during ischemia and reperfusion periods and number of dogs excluded for lethal arrhythmia

Groups	Lethal arrhythmia		No. of excluded dogs	
	Ischemia period (counts)	Reperfusion period (counts)	Vf (counts)	Collateral blood flow (ml/100 g/min)
Control gas	0	23	1	3
H_2 gas	0	5	0	2
H_2 gas + 5HD	0	29	1	3
H_2 gas + Atr	0	27	1	3
Control gas + 5HD	0	28	2	2
Control gas + Atr	1	30	3	2

Incidence of lethal arrhythmia is shown in the included dogs of the present study. H_2 gas group tended to reduce incidence of lethal arrhythmia, however, there were no significant differences among the six groups. Vf = ventricular fibrillation; Abbreviations as in Table 1

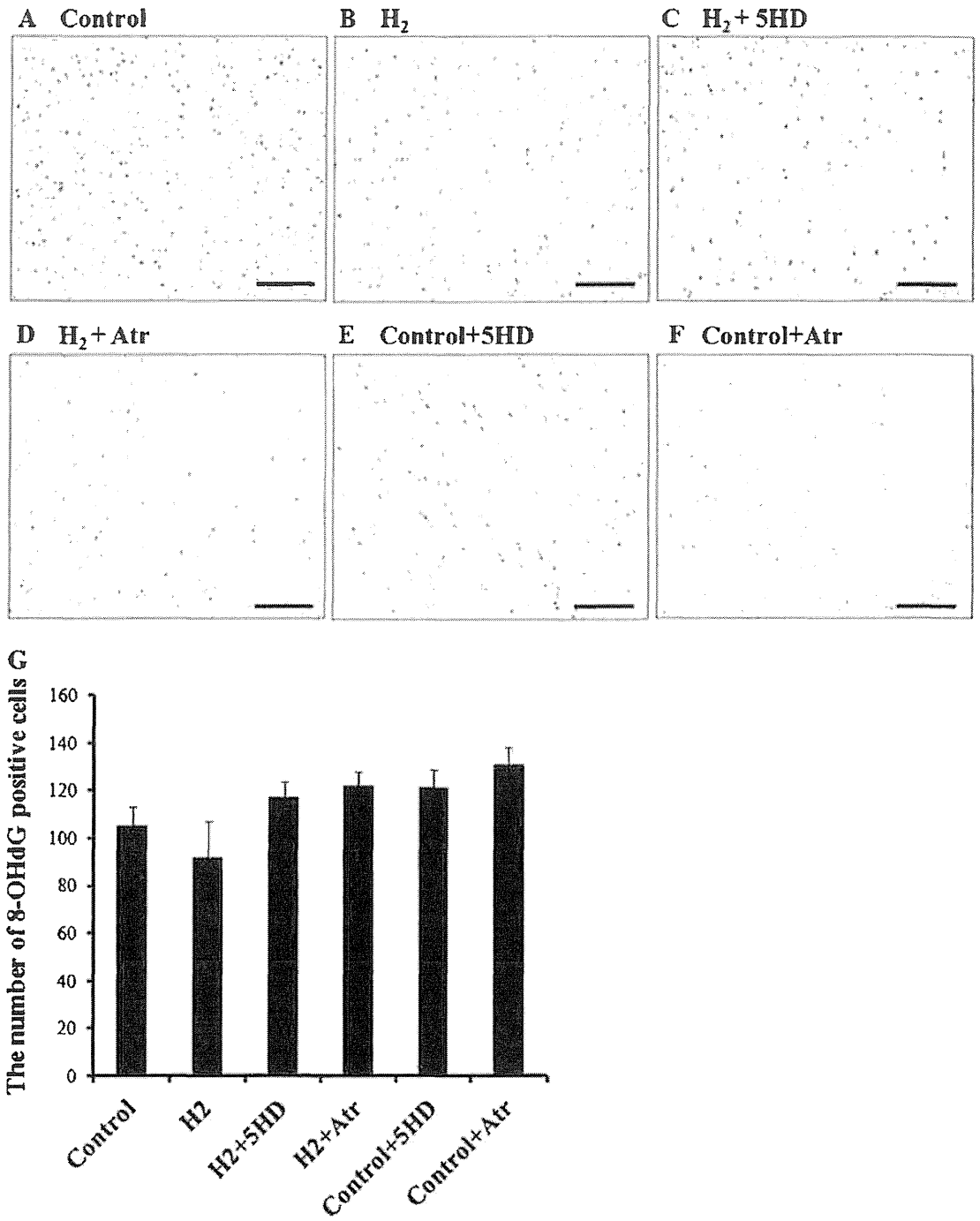

Fig. 4 The number of 8-OHdG positive cells. Representative photos assessed by 8-OHdG immunoreactivity. Staining was localized to nuclei of myocardium (brown) in the control gas (**A**), H_2 gas (**B**), H_2 gas with 5HD (**C**), H_2 gas with Atr (**D**), control gas with 5HD (**E**), and the control gas with Atr groups (**F**) respectively. Scale bar=100 μm. **G** The quantification of 8-OHdG positive cells was expressed per field. There were no significant differences among the six groups. Values are expressed as mean ± SEM (error bars)

did not determine the mechanisms underlying these differences. Since the mechanisms of myocardial necrosis and apoptosis are different [15], our results do not discourage the clinical use of H_2.

On the other hand, we also observed the tendency that H_2 gas mediates the inhibitory effect on reperfusion arrhythmias suggesting that H_2 gas may primarily inhibit reperfusion lethal arrhythmias, however, we cannot deny the

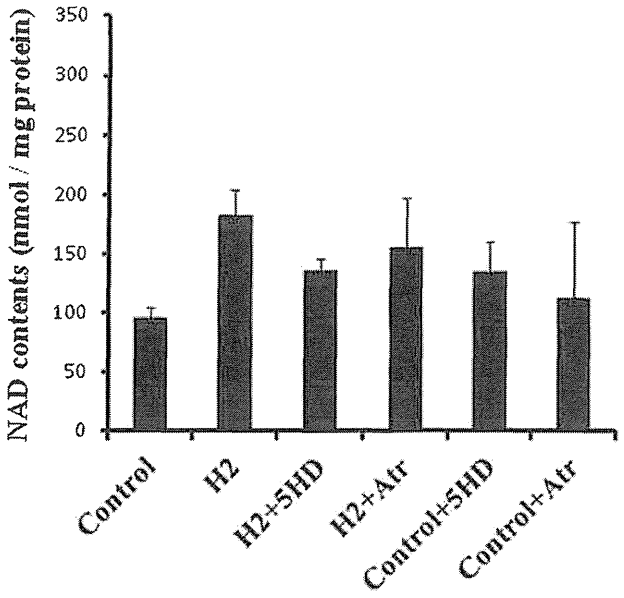

Fig. 5 The myocardial NAD contents. There were no significant differences of myocardial NAD contents among the six groups. Values are expressed as mean ± SEM (error bars)

possibility that this anti-arrhythmic effect of H_2 gas is secondary to the infarct size-limiting effect.

Cellular mechanisms of H_2 gas-induced cardioprotection

H_2 gas is reported to scavenge the detrimental, hydroxyl-radical and peroxynitrate reactive oxygen species without affecting less potent oxygen derived-free radicals or hydrogen peroxide [10]. This may afford cardioprotection by attenuating the end-products of ROS [5, 16–19]. However, this does not necessarily mean that removal of detrimental ROS is the sole mechanism by which H_2 gas induces cardioprotection. Indeed, we found no significant differences in myocardial 8-OHdG immunoreactivity (Fig. 4) among the six groups although there was a trend to lower 8-OHdG positive cells, suggesting that the current dose of H_2 gas may not provide anti-oxidant effects enough to potently reduce infarct size. In turn, we observed the alternative mechanism for H_2 gas to mediate cardioprotection, i.e., the activation of mK_{ATP} followed by the inhibition of mPTP during reperfusion following myocardial ischemia. It would be difficult for chemicals or endogenous substances to physically reach mK_{ATP} upon reperfusion, and the most important endogenous mediator of ischemic preconditioning, adenosine, opens mK_{ATP} via adenosine receptors, Gi proteins, and PKC pathways [20–23]. However, H_2 gas easily penetrates cells and reaches cellular substances and mitochondria [10], suggesting that H_2 gas can reach and activate mK_{ATP}. Another possibility is that H_2 gas activates PKC inside cells, and the activated PKC opens mK_{ATP}. The activation of mK_{ATP} is reported to transmit signals that inhibit mPTP [24–30], which causes potent cardioprotection. An additional finding was that no significant differences were shown in myocardial NAD+ contents although there was a trend to increase in H_2 group. The effects of H_2 gas to modulate either mKATP or mPTP are through a pathway other than NADH dehydrogenase, although there are data showing that the opening of mKATP increases ROS, which modulates mPTP and mediates cardioprotection.

Although we do not understand the precise mechanisms by which H_2 gas opens mK_{ATP}, the evidence in the present study suggests that H_2 gas stimulates intracellular signaling pathways of ischemic preconditioning or postconditioning of cardioprotection [31]. Since H_2 gas is produced in vivo [32], this mechanism may serve as a trigger or mediator of ischemic preconditioning. In turn, it is hard for basic and clinical researchers to translate the fruitful results of ischemic pre- or postconditioning to clinical outcomes. If H_2 gas-induced cardioprotection breaks into the sequels of the signal transduction of ischemic pre- or postconditioning, H_2 gas is likely to be used in clinical situations. Indeed, cyclosporine, which inhibits mPTP, has recently been shown to mediate potent cardioprotection in patients with acute myocardial infarction [9].

Translation to clinical medicine

Before considering the translation of the present results to clinical settings, we need to consider several issues. First, we used 1.3% H_2 gas in the present study. However, since even 0.5% H_2 gas was shown to limit infarct size in previous work [5], 1.3% or even 1% H_2 gas may be sufficient to reduce infarct size in humans. Further, it may be a good idea to use H_2 saline because several studies have shown the cytoprotective effects of H_2 saline [4, 18, 33–38]. Second, we sometimes use carperitide, nicorandil, or nitrate upon reperfusion in patients with AMI as an adjunct therapy, and these drugs might weaken the ability of H_2 gas to limit infarct size. Carperitide and nitrate have been reported to use pathways other than mK_{ATP} [39–41]; however, nicorandil may share this pathway with H_2 gas. However, since neither nicorandil nor H_2 gas fully opens mK_{ATP} channels in vivo, the combination of these two chemicals may be additive or synergistic in limiting infarct size. Third, we observed that inhalation of H_2 gas also tended to reduce the incidence of lethal ventricular arrhythmia such as ventricular tachycardia and Vf. Although we did not precisely investigate the cellular mechanisms whereby H_2 gas limited the incidence of lethal arrhythmia, we assume that the opening of mK_{ATP} and the inhibition of mPTP may be primarily or secondarily involved (Table 2).

Although we need to overcome many issues to translate the present findings, we are encouraged to further

investigate this issue by the fact that we observed H_2 gas-induced cardioprotection in large animals and the mechanism is attributable to the activation of mK_{ATP} followed by the inhibition of mPTP.

Acknowledgements This work was supported by the Grants-in-aid from the Ministry of Health, Labor, and Welfare-Japan (H23-Nanchi-Ippan-22 to M.K.) and Grants-in-aid from the Ministry of Education, Culture, Sports, Science and Technology-Japan (21390251 to M.K.) and Grants from the Japan Heart Foundation and Grants from the Japan Cardiovascular Research Foundation. The authors thank Akiko Ogai for her technical assistance; Hatsue Ishibashi-Ueda for advice about TUNEL staining and Imai Nobuyoshi for his technical assistance with TUNEL staining; Kyoko Shioya for her assistance with animal care; Toshiyasu Asahara and Masaharu Onogi (TAIYO NIPPON SANSO Co.) for providing information about hydrogen.

Conflict of interest The authors declare that they have no conflict of interest.

References

1. Ovize M, Baxter GF, Di Lisa F, et al. Postconditioning and protection from reperfusion injury: where do we stand? Position paper from the Working Group of Cellular Biology of the Heart of the European Society of Cardiology. Cardiovasc Res. 2010;87:406–23.
2. Hausenloy DJ, Baxter G, Bell R, et al. Translating novel strategies for cardioprotection: the Hatter Workshop Recommendations. Basic Res Cardiol. 2010;105:677–86.
3. Kitakaze M, Asakura M, Kim J, et al. Human atrial natriuretic peptide and nicorandil as adjuncts to reperfusion treatment for acute myocardial infarction (J-WIND): two randomised trials. Lancet. 2007;370:1483–93.
4. Sun Q, Kang Z, Cai J, et al. Hydrogen-rich saline protects myocardium against ischemia/reperfusion injury in rats. Exp Biol Med. 2009;234:1212–9.
5. Hayashida K, Sano M, Ohsawa I, et al. Inhalation of hydrogen gas reduces infarct size in the rat model of myocardial ischemia–reperfusion injury. Biochem Biophys Res Commun. 2008;373:30–5.
6. Hausenloy DJ, Ong S-B, Yellon DM. The mitochondrial permeability transition pore as a target for preconditioning and postconditioning. Basic Res Cardiol. 2009;104:189–202.
7. Di Lisa F, Canton M, Carpi A, et al. Mitochondrial injury and protection in ischemic pre- and postconditioning. Antioxid Redox Signal. 2011;14:881–91.
8. Heusch G, Boengler K, Schulz R. Inhibition of mitochondrial permeability transition pore opening: the Holy Grail of cardioprotection. Basic Res Cardiol. 2010;105:151–4.
9. Piot C, Croisille P, Staat P, et al. Effect of cyclosporine on reperfusion injury in acute myocardial infarction. N Engl J Med. 2008;359:473–81.
10. Ohsawa I, Ishikawa M, Takahashi K, et al. Hydrogen acts as a therapeutic antioxidant by selectively reducing cytotoxic oxygen radicals. Nat Med. 2007;13:688–94.
11. Kitakaze M, Node K, Minamino T, et al. Role of activation of protein kinase C in the infarct size-limiting effect of ischemic preconditioning through activation of ecto-5′-nucleotidase. Circulation. 1996;93:781–91.
12. Mori H, Haruyama S, Shinozaki Y, et al. New nonradioactive microspheres and more sensitive X-ray fluorescence to measure regional blood flow. Am J Physiol. 1992;263:H1946–57.
13. Kitakaze M, Node K, Minamino T, et al. Role of nitric oxide in regulation of coronary blood flow during myocardial ischemia in dogs. J Am Coll Cardiol. 1996;27:1804–12.
14. Kitakaze M, Node K, Takashima S, et al. Role of cellular acidosis in production of nitric oxide in canine ischemic myocardium. J Mol Cell Cardiol. 2001;33:1727–37.
15. Kung G, Konstantinidis K, Kitsis RN. Programmed necrosis, not apoptosis, in the heart. Circ Res. 2011;108:1017–36.
16. Fukuda K-I, Asoh S, Ishikawa M, Yamamoto Y, Ohsawa I, Ohta S. Inhalation of hydrogen gas suppresses hepatic injury caused by ischemia/reperfusion through reducing oxidative stress. Biochem Biophys Res Commun. 2007;361:670–4.
17. Buchholz BM, Kaczorowski DJ, Sugimoto R, et al. Hydrogen inhalation ameliorates oxidative stress in transplantation induced intestinal graft injury. Am J Transplant. 2008;8:2015–24.
18. Cai J, Kang Z, Liu K, et al. Neuroprotective effects of hydrogen saline in neonatal hypoxia–ischemia rat model. Brain Res. 2009;1256:129–37.
19. Li J, Wang C, Zhang JH, Cai JM, Cao YP, Sun XJ. Hydrogen-rich saline improves memory function in a rat model of amyloid-beta-induced Alzheimer's disease by reduction of oxidative stress. Brain Res. 2010;1328:152–61.
20. Tsukamoto O, Asanuma H, Kim J, et al. A role of opening of mitochondrial ATP-sensitive potassium channels in the infarct size-limiting effect of ischemic preconditioning via activation of protein kinase C in the canine heart. Biochem Biophys Res Commun. 2005;338:1460–6.
21. Hanley P, Daut J. K channels and preconditioning: a re-examination of the role of mitochondrial K channels and an overview of alternative mechanisms. J Mol Cell Cardiol. 2005;39:17–50.
22. Kitakaze M, Minamino T, Node K, et al. Role of activation of ectosolic 5′-nucleotidase in the cardioprotection mediated by opening of K+c channels. Am J Physiol. 1996;270:H1744–56.
23. O'Rourke B. Myocardial K(ATP) channels in preconditioning. Circ Res. 2000;87:845–55.
24. Hausenloy DJ, Maddock HL, Baxter GF, Yellon DM. Inhibiting mitochondrial permeability transition pore opening: a new paradigm for myocardial preconditioning? Cardiovasc Res. 2002;55:534–43.
25. Lim SY, Davidson SM, Hausenloy DJ, Yellon DM. Preconditioning and postconditioning: the essential role of the mitochondrial permeability transition pore. Cardiovasc Res. 2007;75:530–5.
26. Murata M, Akao M, O'Rourke B, Marban E. Mitochondrial ATP-sensitive potassium channels attenuate matrix Ca2+ overload during simulated ischemia and reperfusion: possible mechanism of cardioprotection. Circ Res. 2001;89:891–8.
27. Hausenloy DJ. Preconditioning protects by inhibiting the mitochondrial permeability transition. AJP Heart Circ Physiol. 2004;287:H841–9.
28. Costa ADT. The mechanism by which the mitochondrial ATP-sensitive K+ channel opening and H2O2 inhibit the mitochondrial permeability transition. J Biol Chem. 2006;281:20801–8.
29. Juhaszova M, Zorov DB, Kim SH, et al. Glycogen synthase kinase-3beta mediates convergence of protection signaling to inhibit the mitochondrial permeability transition pore. J Clin Invest. 2004;113:1535–49.
30. Terashima Y, Sato T, Yano T, et al. Roles of phospho-GSK-3β in myocardial protection afforded by activation of the mitochondrial KATP channel. J Mol Cell Cardiol. 2010;49:762–70.
31. Heusch G, Boengler K, Schulz R. Cardioprotection: nitric oxide, protein kinases, and mitochondria. Circulation. 2008;118:1915–9.
32. Hammer HF. Colonic hydrogen absorption: quantification of its effect on hydrogen accumulation caused by bacterial fermentation of carbohydrates. Gut. 1993;34:818–22.